

Application of a Heat Conductor Technique in the Production of Single-Crystal Turbine Blades

DEXIN MA and A. BÜHRIG-POLACZEK

The heat conductor (HC) technique was applied in the production of single-crystal turbine blades with the aim of reducing grain defects originating from a geometrical feature. Because of its excellent thermal-physical properties, graphite is recommended as HC material. Numerical simulation and temperature measurements were able to prove that the thermal condition in the shroud region of turbine blades is significantly improved for single-crystal growth. The reduction in thermal undercooling entirely eliminated the high-angle boundary, resulting in an effective improvement in the casting quality of components.

DOI: 10.1007/s11663-009-9274-7

© The Minerals, Metals & Materials Society and ASM International 2009

I. INTRODUCTION

SINGLE-CRYSTAL solidification of turbine blades for advanced gas turbines is a key technology for the production of reliable and high-efficiency gas turbines. The excellent properties of single crystals originate from the absence of grain boundaries, which eliminate sites liable to result in crack nucleation under thermomechanical fatigue conditions. Under creep conditions, the absence of grain boundaries not only removes the sites liable to host fracture initiation but also to remove a potential mechanism for high-temperature deformation, in particular grain boundary sliding.^[1] Because of ever-increasing demands on casting quality, the production of single-crystal turbine blades has been thoroughly investigated. Unfortunately, control of the industrial casting process is still not to a satisfactory level, so that a significant number of the components produced have to be rejected because of the grain defects, which form a high-angle boundary with the primary crystal.^[2]

Grain defects mostly occur as a consequence of the preferred solidification of geometrical features of the component. Experimental investigation has shown that the macroscopic curvature of the liquidus isotherm becomes markedly concave while traversing extreme enlargements in the cross section of the component, *e.g.*, transition from the blade portion to the shroud portion.^[3] This leads to the formation of an isolated, thermally undercooled region of melt, which may lead to heterogeneous nucleation and hence the formation of stray grains.

As blade designs become more complex and the demand for larger single-crystal castings dramatically increases, the formation of grain defects caused by geometrical features becomes an increasingly serious challenge. This key problem cannot be effectively

overcome by conventional process modification, such as optimization of withdrawal rate or baffle design.

The authors have recently developed a heat conductor (HC) technique to improve the thermal condition at the transition point and thus to suppress stray grain formation at the extremities of the platform.^[4] The assumption was, as shown in Figure 1(a), that a hot spot exists at the inner corner of the cross-sectional transition (position A), resulting from the poor local cooling condition. This hot spot hinders single-crystal growth from the blade portion into the platform. On contrast, the outer corner (position B) cools more rapidly because the local shell mold is much thinner. As a result, because of the concave curvature of the liquidus isotherm, the temperature at position B falls faster below the liquidus temperature, and the dendrite tips of the primary crystal are unable to reach this isolated undercooled region, where stray grains eventually occur. In the HC technique, as shown in Figure 1(b), a heat conductor is inserted close to the critical position A to improve the local cooling condition. The other end of the HC protrudes from the mold to ensure effective heat radiation into the cold environment in the Bridgman-furnace chamber. Efficient heat extraction minimizes the hot spot at position A. This promotes the successful transition of single-crystal growth from the blade body into the extremity B of the platform before local undercooling exceeds the critical value for heterogeneous nucleation.

The effectiveness of the HC technique has been confirmed in principle in previous projects by using a simple geometry with an abrupt section enlargement.^[5] The objective of the present work is to apply the HC technique to the production of turbine blades and to confirm the effectiveness of the technique.

II. EXPERIMENTAL

A. Blade Geometry and Mold Preparation

The test component selected for these experiments was an actual turbine blade whose shroud has both

DEXIN MA, Research Scientist, and A. BÜHRIG-POLACZEK, Director, are with the Foundry Institute, RWTH University Aachen, 52072 Aachen, Germany. Contact e-mail: d.ma@gi.rwth-aachen.de
Manuscript submitted January 20, 2009.
Article published online August 14, 2009.

abrupt cross-section enlargement from the aerofoil and an overhanging outer corner (Figure 2(a)). This design was selected to provide a typical geometrical feature that is most prone to thermal undercooling and, hence, to subsequent grain defects. In this case, the application of the HC technique is especially desirable.

The ceramic shell molds were produced by a modified investment casting procedure, the principles of which are shown in Figures 2(a) to (d). After finishing the first ceramic layer on the wax pattern, as in standard investment casting, the graphite HC was bonded at the locations selected using a ceramic binder. By repeating the procedure of dipping in ceramic slurries and sanding with fused alumina, the shell molds were produced to the final thickness (Figure 2(d)). In parallel, the exterior of the HC was cleaned with a toothbrush to maintain it free of ceramic accumulation. Figure 2 shows the principle of shell mold manufacture for a single blade.

In fact, the blades were cast in clusters, in which the blades were arranged in a circle around a central rod (see also the mold cluster in Figure 3). One half of the blades in each cluster were bonded with HC to investigate the effectiveness of this new technique in comparison with the halves with no HC.

After dewaxing in a steam autoclave, the shell molds were subsequently sintered at 1200 °C in a closed steel box in a firing furnace (Figure 3). To protect the inserted graphite HC against oxidation, some pieces of waste graphite were placed in the box. This protective measure has been proven to ensure that no vacuum and inert gas atmosphere is necessary.

B. Selection of HC Material

Graphite is used as HC material because of its excellent thermal physical properties and very good

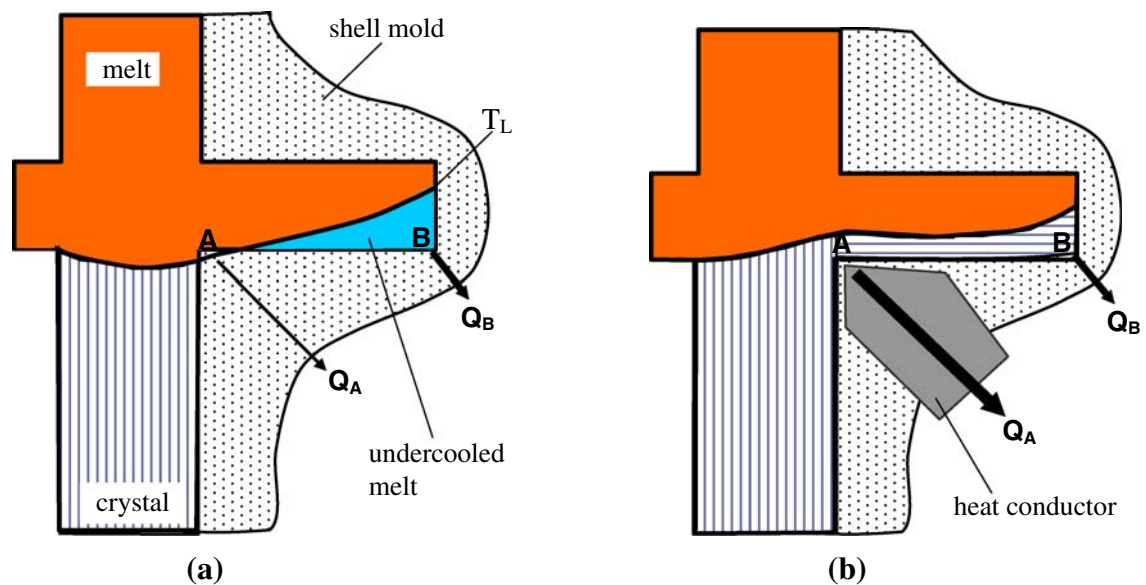


Fig. 1—(a) Schematic diagram shows the formation of the undercooled zone at the platform extremity B. (b) Schematic diagram of the HC technique for reducing undercooling at B by improving the cooling condition at region A.

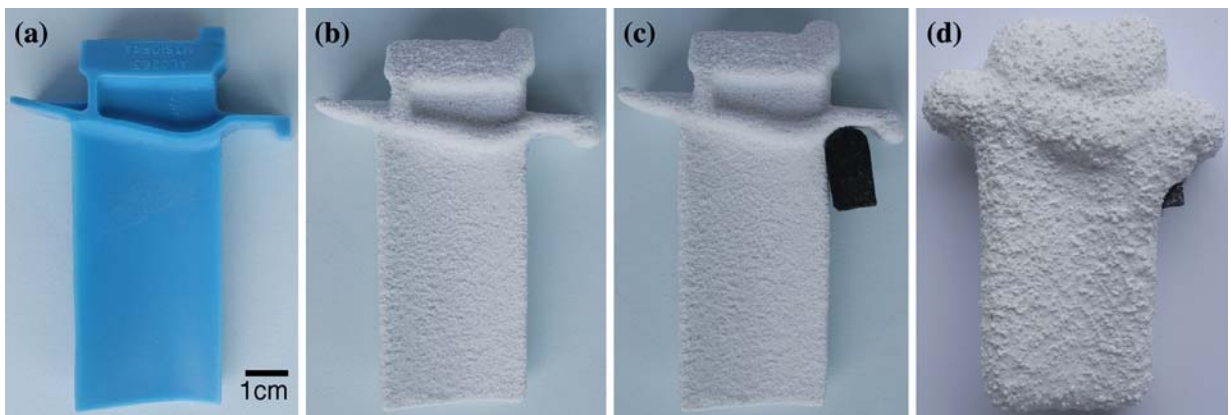


Fig. 2—Procedure of shell mold manufacture for inserting HC: (a) wax model; (b) after first layer; (c) attachment of HC; and (d) shell mold finished for dewaxing.

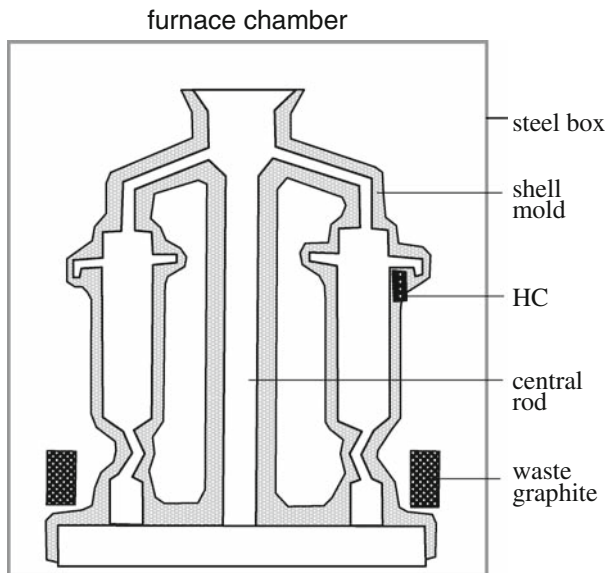


Fig. 3—Schematic diagram of firing shell mold in a furnace chamber.

resistance against high temperature in vacuum. Figure 4 shows the relevant thermophysical properties of the used graphite in comparison with those of the superalloy and ceramic mold (Al_2O_3). The heat conductivity of graphite is about 30 times as high as that of ceramic (Figure 4(a)). Thus, it can be estimated that the HC can extract correspondingly such more heat than the shell mold under the same condition. By selecting a suitable size of HC, it can extract enough of the heat from the critical position and effectively reduce the hot spot from hindering the single-crystal growth. The volumetric heat content ρC_p (ρ = density and C_p = heat capacity) for graphite is lower than for ceramic material (Figure 4(b)). This means, compared with ceramic mold, less heat is stored in the HC during the heating process, which has to be additionally extracted during the solidification process. Graphite also has a high emission coefficient ε (Figure 4(c)), which ensures effective heat radiation into the cold chamber of the Bridgman-furnace. For these reasons, graphite becomes a very suitable material for the HC technique.

C. Casting with Temperature Measurement

To measure the development of the liquidus isotherm while traversing the critical shroud areas, thermocouples were placed at exactly defined positions. For this purpose, the ceramic sheaths were inserted into the wax patterns before dipping and sanding (Figure 5(a)). After dewaxing and firing, the thermocouples of type “B” (Pt-30 pct Rh/Pt-6 pct Rh) were installed into the ceramic sheaths in the shell mold (Figure 5(b)). The casting experiments were performed as a standard Bridgman process. The alloy used in this experiment is a Ni-based, single-crystal superalloy CMSX-6 (Cr 9.8, Co 5.0, Mo 3.0, Al 4.8, Ti 4.7, and Ta 2.0 in wt pct) with a liquidus temperature of about 1321 °C.^[6] A heater temperature of $T_H = 1530$ °C, a pouring temperature

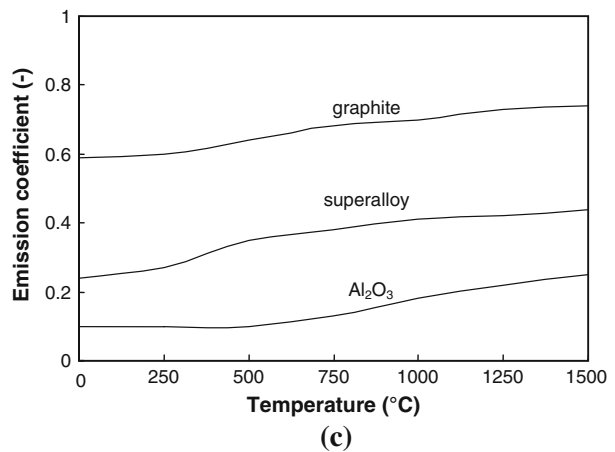
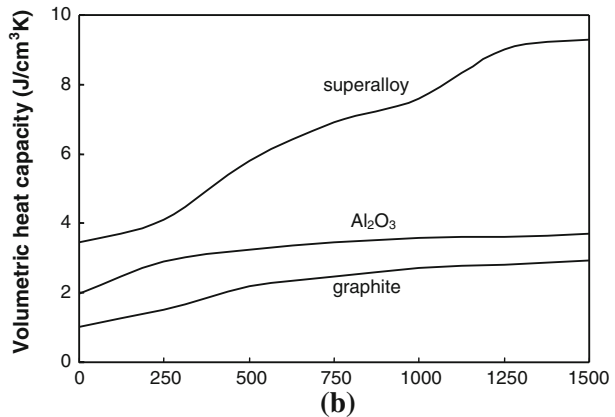
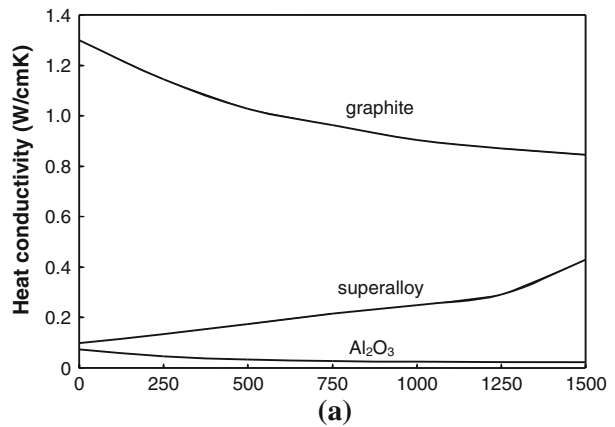


Fig. 4—Thermophysical properties of the materials used (graphite, superalloy, and ceramic).

of $T_P = 1500$ °C and a withdrawal velocity of $V = 3$ mm/min are standard process parameters of the Bridgman process.

D. Computer Simulation

Ahead of casting experiments, numerical simulation was applied to predict the possible impact of HC on solidification in the shroud region. Macroscopic solidification modeling was executed using the finite element code CASTS,^[7,8] a well-established tool for simulation

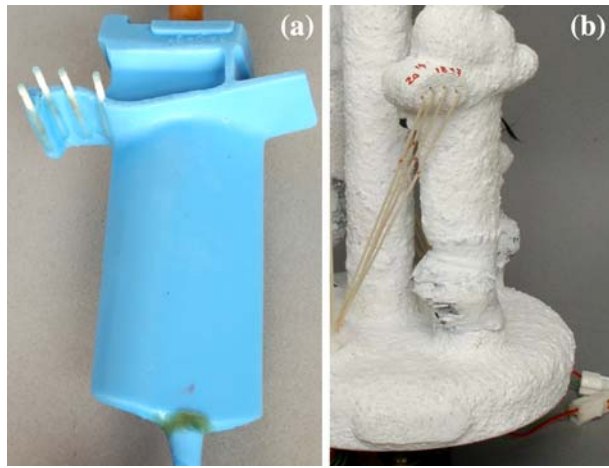


Fig. 5—Placement of alumina insulator sheaths in wax pattern (a) and instrumentation of thermal couples in mold (b).

of the Bridgman process. CASTS fully describes the heat transfer balance in the vacuum furnace, including calculation of view factor radiation. The experimental setup, including furnace, blades, and shell mold with HC, was generated as a finite element method (FEM) mesh. The geometric data were transformed into an appropriate file format, including additional elements at the interface between different materials. These elements realize the interfacial heat flow. The temperature-dependent thermophysical properties, including those shown in Figure 4, were read. The initial and boundary condition were set to be the same as the experiment (i.e., $T_H = 1530$ °C, $T_P = 1500$ °C, and $V = 3$ mm/min). All information was stored in a command file. Using both the modified geometry and the command file, the main program evaluated iteratively the temperature evolution, taking into account the release of latent heat and position-dependent viewing factors. The transient temperature distribution as well as the macroscopic shape and progress of the liquidus isotherm were later visualized using the CASTS-tool COLOR3D.

III. RESULTS AND DISCUSSION

A. Solidification Simulation

As stated, numerical simulation was performed ahead of the casting experiments. Figure 6 shows the simulated temperature development in two shrouds, without (left) and with (right) application of HC, respectively. Because of the symmetrical arrangement, both blades have the same external thermal condition. The difference in temperature history can then be attributed solely to the application of HC.

At time t_1 , the temperature at the outer corner of both shrouds decreases below T_L and the effect of HC has not yet been clearly revealed. At times t_2 and t_3 , the isolated outer corner of the original shroud becomes increasingly undercooled. In contrast, the bonded HC acts as a heat sink for the casting and effectively removes the hot spot at the inner corner of the shroud. The undercooled

extremity soon comes into contact with the primary crystal in the blade body, from which an epitaxial crystal transition should be introduced. With no HC application, the undercooled extremity remains thermally isolated for a much longer time, over which local undercooling continues to increase.

The simulation result clearly shows that thermal undercooling at the shroud extremities is unavoidable and, at the same time, the effectiveness of the HC technique. Heat extraction from the cross-sectional transition is significantly improved. The solidification front in the blade body can move into the shroud more quickly, before the melt in the outer corner becomes deeply undercooled. From this prediction, it can be assumed that the risk of heterogeneous nucleation of stray grain is dramatically reduced, although it remains impossible to eliminate undercooling entirely.

The simulation was performed under equilibrium conditions and thermal undercooling at the extremities was practically underestimated.^[9] A consideration of the kinetics of dendrite growth, especially the transition from vertical to lateral growth, as well as nucleation kinetics, leads to the conclusion that the thermal undercooling measured will be greater than predicted by the simulation.

B. Temperature Measurement

Figure 7 shows the cooling curves measured by the thermocouples at the marked positions on the shrouds. With no HC (Figure 7(a)), the extremity of the platform (point 4 and 3) cools more deeply than the inner point 1. The measurement shows a maximum undercooling ΔT_M of approximately 29 °C below an approximate T_L of 1321 °C at the outer corner (thermocouple 4) prior to the start of local solidification. The corresponding undercooling time Δt_M is approximately 244 s.

With the application of HC, a notable change in the cooling curves was measured, indicating a significant improvement in cooling condition at the inner corner of the platform (Figure 7(b)). The temperature at point 1 becomes even lower than that of point 2. Approximately 45 s after point 4, point 1 had cooled to T_L , whereas with no HC the same cooling took approximately 120 s, as shown in Figure 7(a). Thus, the undercooled zone at the extremity is no longer so isolated from the solidification front in the blade body. The maximum undercooling at point 4, ΔT_M , and the corresponding undercooling time Δt_M are reduced from approximately 29 °C to 18 °C and 244 s to 150 s, respectively. Since the probability of grain nucleation in an alloy melt is dependent on the value of ΔT_{max} and Δt_{max} , the conclusion must be that the notable reduction achieved by application of HC will significantly reduce the probability of stray grain formation.

From the temperature measurement, it is possible to reconstruct the liquidus isotherm passing through the platform (Figure 8). With no HC, a significantly concave-shaped isotherm is obtained (except on the outer side where the isotherm becomes convex because in a position favorable to radiation by the heaters). Through the application of HC, the T_L -isotherm in the platform

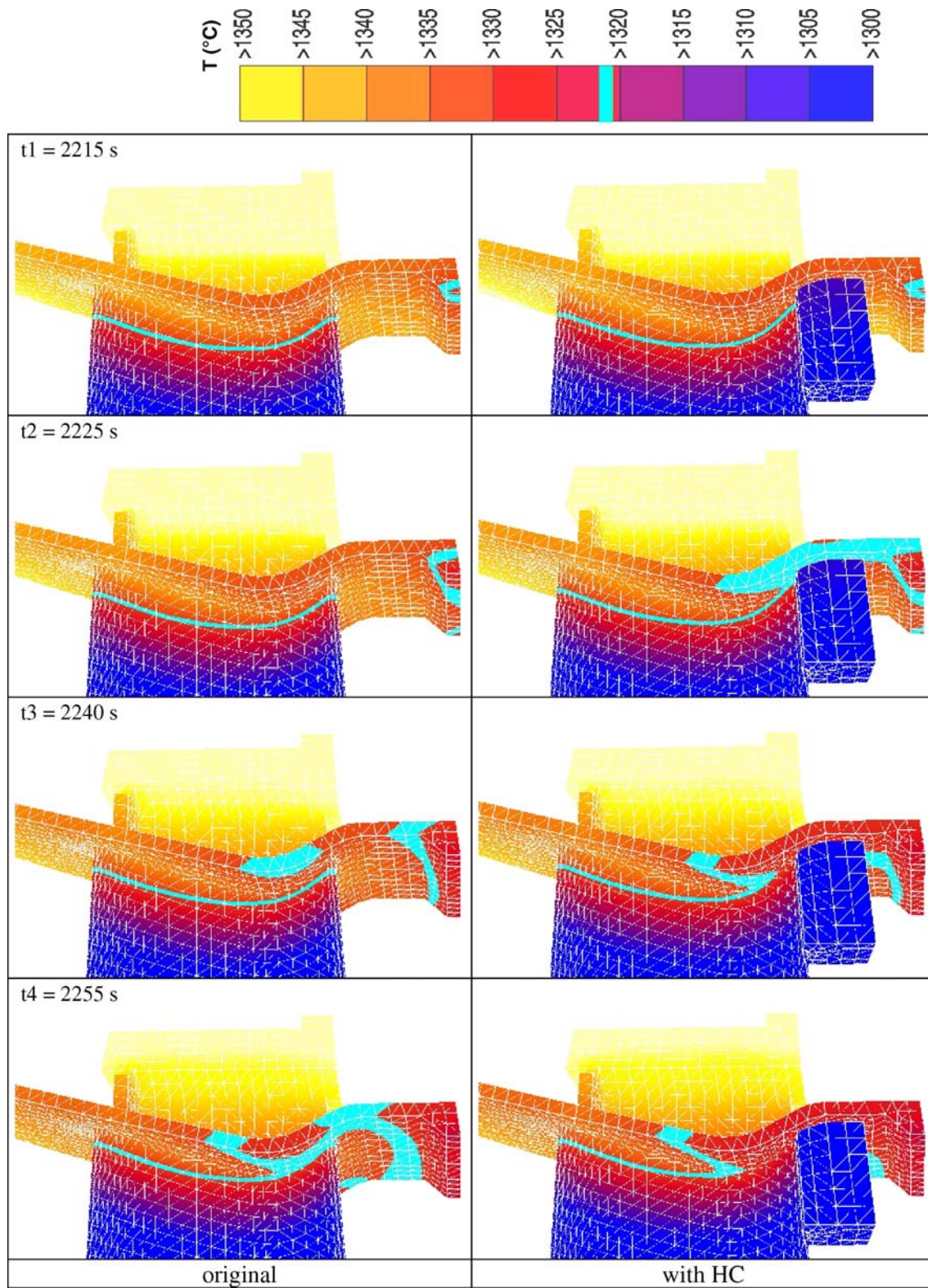


Fig. 6—Simulated temperature development in the blade platform (left: without HC, right: with HC).

becomes significantly smoothed. At the time point $t_1 = 2105$ s, the T_L -isotherm reaches the inner corner of the platform (point 1). With no HC, this was delayed to $t_2 = 2190$ s, approximately 85 s later, resulting in an

increasingly undercooled extremity. Thus, as stated, the application of HC can significantly reduce the time and the extent of the isolated undercooling and, consequently, the possibility of grain defects.

C. Metallographic Examination

In this project, 16 blades were cast, the halves of which were applied with HC, of which one is shown in Figure 9. After shakeout from the mold, the blades were

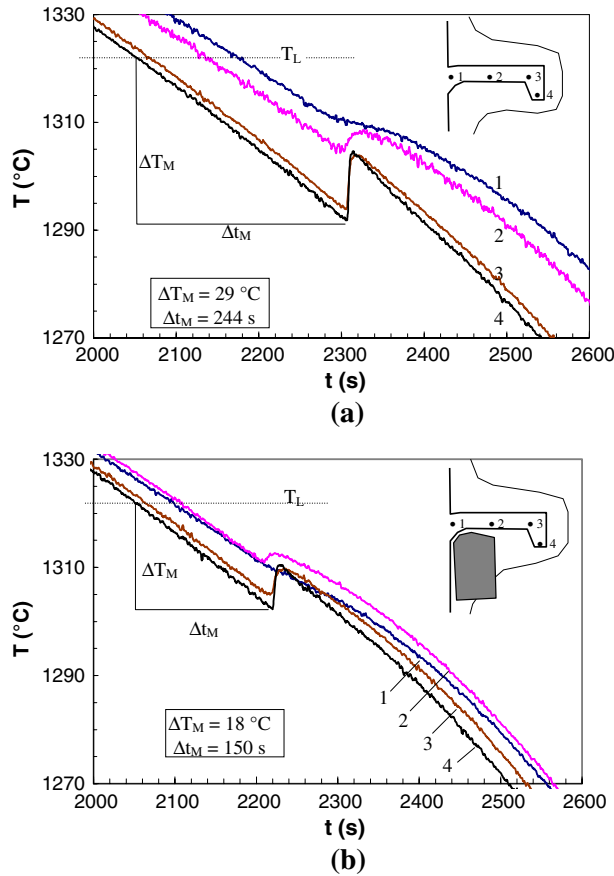


Fig. 7—Cooling curves measured in the shroud of the blade (*a*: without HC, *b*: with HC).

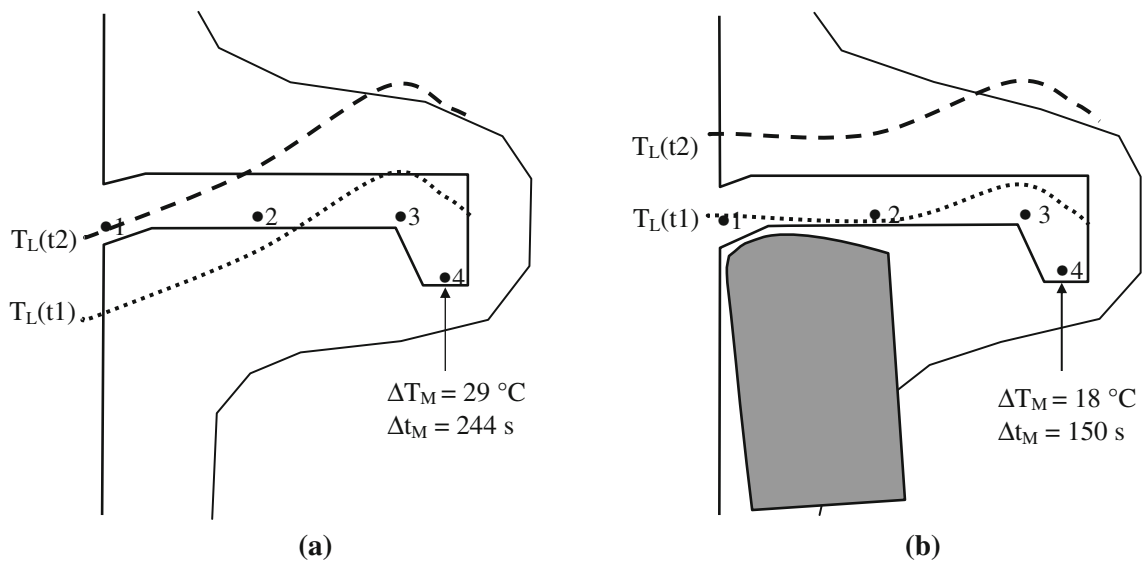


Fig. 8—Reconstructed liquidus-isotherm (T_L) when passing through the blade shroud (*a*: without HC, *b*: with HC). ($t_1 = 2105$ s, $t_2 = 2190$ s).

macroscopically etched to reveal the grain and dendrite structure at the surface. Several types of grain defects, such as stray grains and low-angle boundaries, were easily visible. It was found that the grain structure defects occur only in the shroud region, whereas the blade bodies were defect-free. To reveal more about the microstructure in the shroud region, the shrouds of all blades were sectioned for metallographic investigation. To evaluate the degree of defect and, hence, to



Fig. 9—Photograph of a blade with attached HC after shakeout from the mold.

determine casting quality, the cast structures were classified into four categories as follows:

1. *Class 1: Single-Crystal Structure Without Grain Defect*

This class of structure shows no grain boundaries on the etched surface, as shown in Figure 10(a). From microscopic observation of the shroud section (Figure 10(b)), including the overhang (Figure 10(c)), all dendrites are orientated in the same direction. This structure was obtained practically only by application of HC. The single-crystal growth was sequentially transferred from blade body to the shroud extremities. Because of the decrease in undercooling, dendrite growth was less accelerated. This permits orderly and stable growth of the columnar dendrite structure with a consistent orientation, instead of an intersected dendrite network.

This typical single-crystal structure is desirable for customers, but it is almost impossible to realize for shroud geometries of this kind unless the HC technique is applied.

2. *Class 2: Single Crystal with Low-Angle Boundaries (LABs)*

On the etched surface, the weak grain boundaries with low-angle boundaries can be identified (Figure 11(a)). The dendrite structure, as shown in Figures 11(b) and (c), is finer than that shown in Figure 10. This can be attributed to the greater velocity of dendrite growth resulting from the greater melt undercooling. The

orientations of dendrite arrays are in principle identical because they originate from the same primary crystal. However, rapid dendrite growth into the increasingly undercooled melt is not successive. Subsequent intersection of different dendrite branches reveals low-angle grain boundaries, as shown bottom left in Figure 11(c).

Low-angle boundaries have no adverse effects on properties,^[1,10] so that the blades of quality class 2 are acceptable.

3. *Class 3: Interdendritic Multiple Grains*

These defects are indistinct on the surface except for some groups of fine spots (Figure 12(a)). In the interior of the overhanging parts, however, fine equiaxed grains were observable (Figures 12(b) and (c)). From macroscopic observation, the base structure still resembles a single crystal because of the identical alignment of dendrite trunks. Microscopic investigation reveals fine equiaxed grains between the dendrite trunks. The size of the equiaxed grains was comparable with the secondary arm spacing of the dendrites. The existence of dendrite trunks means that initial nucleation can be excluded. The only mechanism for the formation of the misoriented grains seems to be the fragmentation of secondary dendrite arms during local solidification. This structural defect is observed only within the shrouds with no HC, because of greater undercooling in the shroud extremities. Dendrite growth could still advance from the primary single crystal into the overhang before an initial grain nucleation occurred. However, rapid crystal growth into the greatly undercooled melt first results

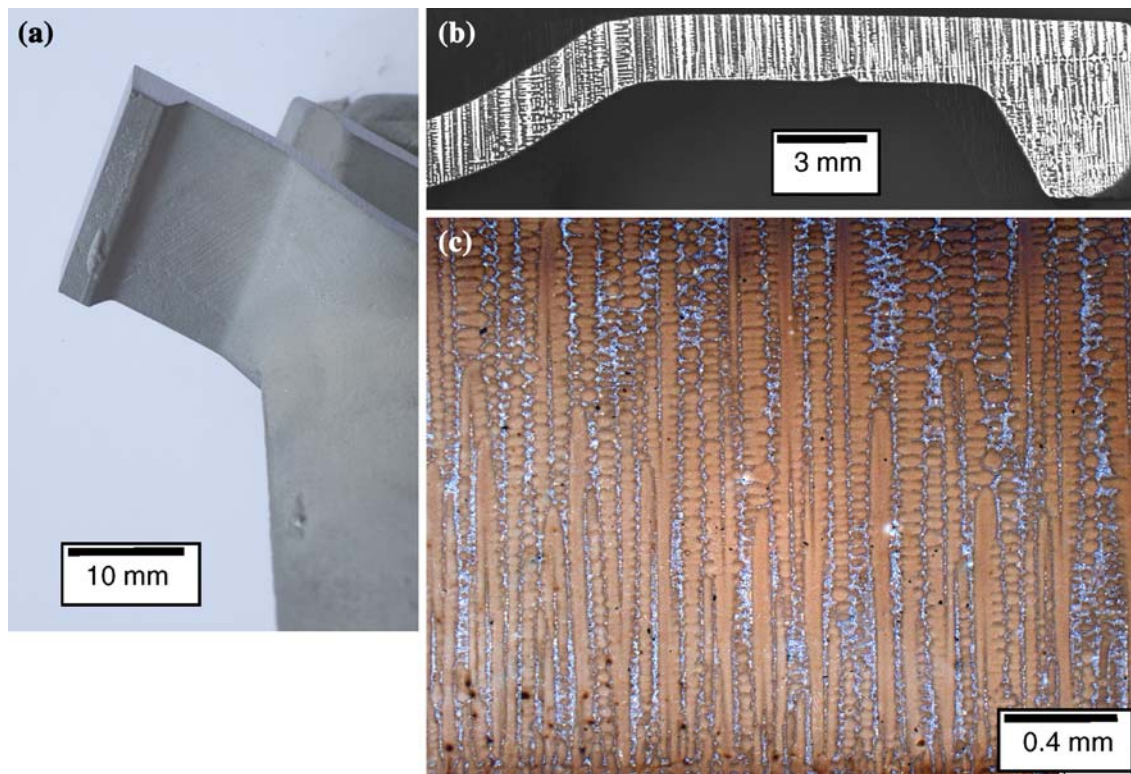


Fig. 10—Cast structure of class 1: single crystal without defect.

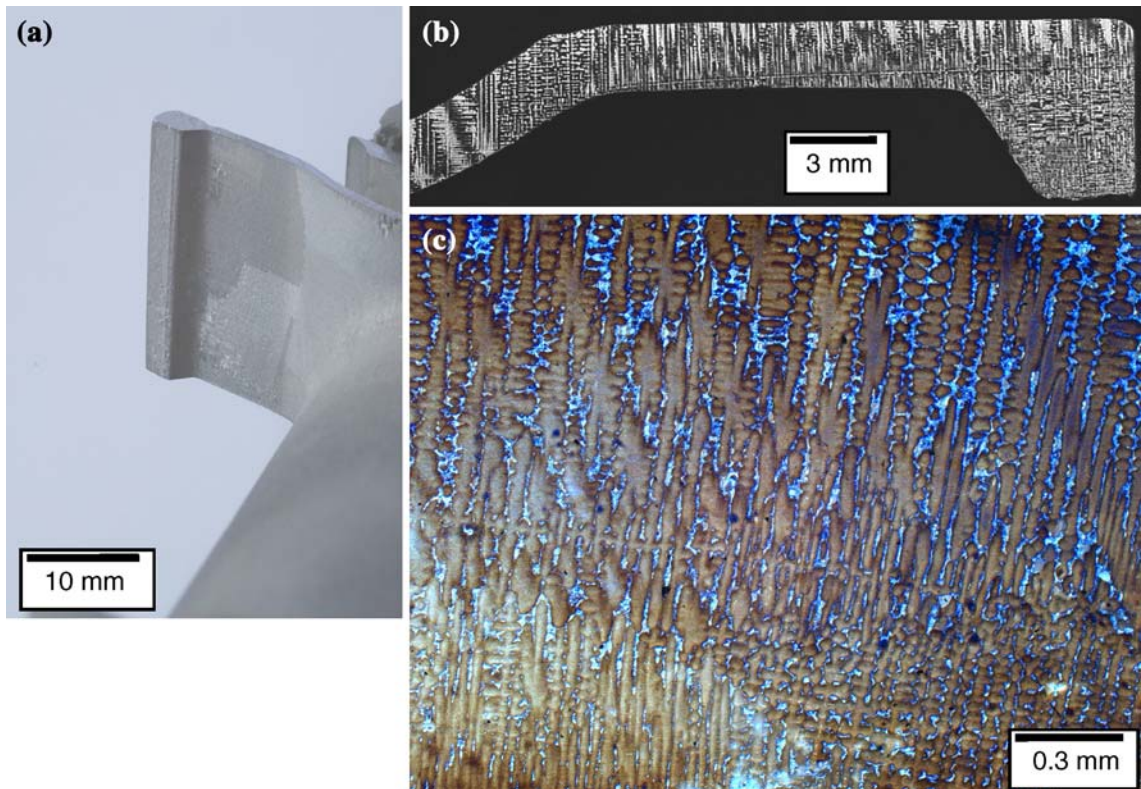


Fig. 11—Cast structure of class 2: single crystal with low-angle grain boundary.

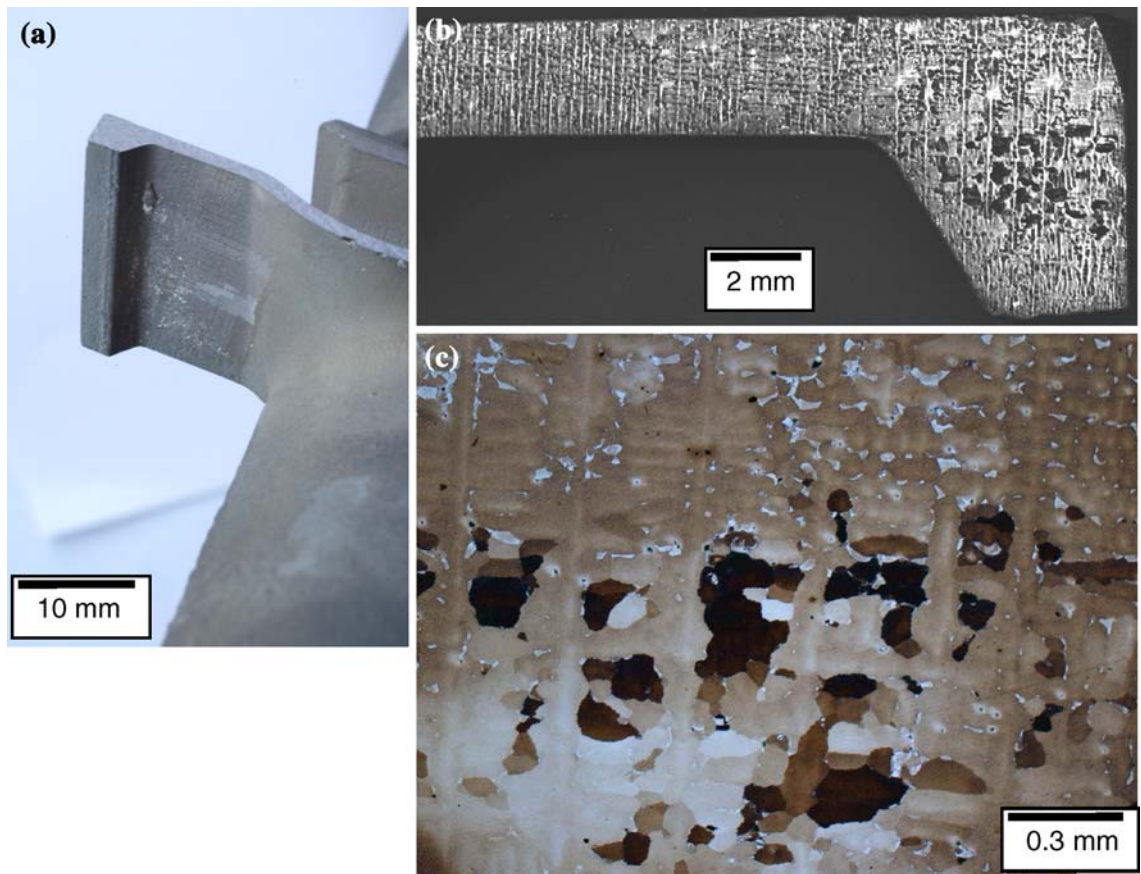


Fig. 12—Cast structure of class 3: interdendritic micro-equiaxed grains.

in a dendrite framework of thin primary/secondary arms. The roots of the dendrite arms are especially thin and weak so that partial remelting can take place during the subsequent coarsening process, starting with recalescence upon the sudden release of latent heat. Because of drift and deflection, the broken arms become new fine grains with orientations different from their parent trunks. During this procedure, no heterogeneous nucleation occurs.

As found in previous research at the Foundry Institute,^[11] the superalloy CMSX 6 is highly undercoolable, for which a maximum undercooling of approximately 80 K is achievable. However, above a critical undercooling of about 30 K, instead of the dendrite structure, a fine equiaxed grain structure occurs. The interdendritic equiaxed grains observed in the present work should be a transition structure slightly inferior to the critical undercooling because measurement in this region reveals an undercooling of approximately 29 °C (Figures 7(a) and 8(a)). In this structure, the dendrite trunks are still “single crystal,” but the interdendritic grains are misoriented from the base crystal and thus destroy the local monocrystallinity. Therefore, thermal undercooling should be limited even if the alloy provides a high undercooling capacity in ceramic molds.

This structure is somewhat similar to freckles, which is another familiar grain defect.^[12] Both appear as interdendritic, fine equiaxed grains and are attributed to the fragmentation of secondary dendrite arms during solidification. However, there are obvious differences: Freckles occur as long chains of equiaxed grains on the surface of the component. In this investigation, the distribution of fine grains in the shroud extremities is found to be random. Although a reasonable explanation for the formation of freckles is offered by thermosolutal convection driven by a density inversion, investigation is

needed to understand the formation mechanism for the interdendritic grains found in the present investigation.

4. Class 4: Heterogeneous Stray Grain

This is a well-known grain defect at shroud extremities. Because of high undercooling, heterogeneous nucleation occurs ahead of the primary single-crystal growth, resulting in the formation of coarse stray crystals. High-angle grain boundaries are apparent on the surface and sections (Figures 13(a) and (b)). Such casting defects render the blades useless for engineering purposes and need to be avoided at all costs.

The examination of the as-cast structure shows that the shroud portion is very prone to grain defect formation because of geometrical discontinuity and subsequent, isolated undercooling. However, this can be improved by application of the HC technique. Table I and Figure 14 show results of the examination of the blades cast in this study. The quality of the blades

Table I. Classification of Cast Blades

		Original	With HC
Number of blade	class 1 (defect-free)	1	4
	class 2 (minor defect)	2	4
	class 3 (middle defect)	3	0
	class 4 (large defect)	2	0
Average quality class		2.75	1.5
Acceptable rate (class ≤ 2)		0.375 (3/8)	1 (8/8)
Reject rate (class ≥ 3)		0.625 (5/8)	0 (0/8)

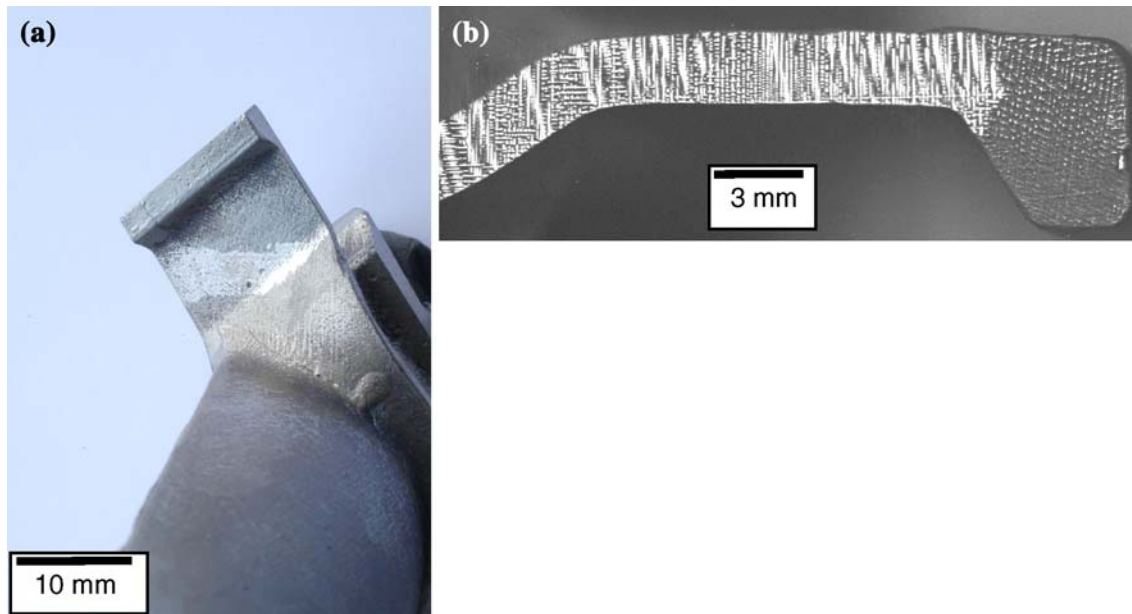


Fig. 13—Cast structure of class 4: heterogeneous stray grain.

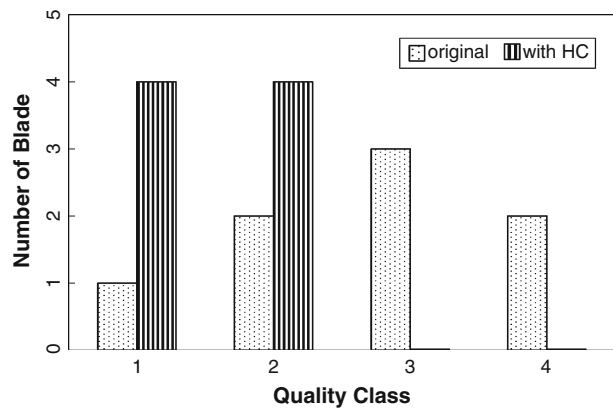


Fig. 14—Diagram of classification of cast blades without and with HC.

with no HC shows a scattered distribution over classes 1 to 4, with a weighted average of 2.75. In contrast, blades with HC have a quality of either class 1 or 2, with an average of 1.5.

In principle, blades of quality class 1 (defect-free) are desirable and those of class 2 (with low-angle boundaries) are also acceptable for customers. In contrast, blades of class 3 and 4 are rejects, since high-angle boundaries and multiple boundaries are obvious sources of weakness. These defects are particularly pernicious since single-crystal formulations do not contain the grain boundary strengtheners found in conventional alloys. In such cases, the supposedly single-crystal alloys will be even weaker than their conventionally cast counterparts and the property deficit relative to the expected single-crystal properties can be catastrophic.^[1]

As shown in Table I, by applying the HC technique, the rate of acceptable cast blades was improved from 37.5 pct to 100 pct, or expressed differently, the reject rate was reduced from 62.5 pct to 0. This provides firm evidence of the effectiveness of the HC technique in reducing grain defects originating from geometrical features.

D. Technical Feasibility of Graphite HC

The HC technique is easy to apply. The technique necessitates no changes to the existing Bridgman setup, only a slight modification to shell mold manufacture. During dewaxing, firing, and casting, no crack or other defects on the shell molds resulting from the attached HCs were detected. This is because the coefficient of thermal expansion of graphite is negligibly low. Since graphite is inexpensive and can be easily shaped to the dimension required, the additional cost is insignificant. Moreover, graphite HCs are reusable. Thus, the benefit of applying the HC technique is high cost-effectiveness.

Once established, the HC technique can be optimized by modification focusing on HC size and geometry and on positioning relative to the components. Additional thermal insulation of the shell molds at the platform extremities will further suppress local undercooling and stray grain formation. The HC technique can be applied together with liquid metal cooling (LMC)^[13,14] and gas

cooling casting (GCC) processes,^[15,16] where the inhomogeneity of heat extraction from the geometrical feature is even more marked. Because of the effective cooling of the HC exterior by liquid metal or inert gas flow, more of the potential provided by this technique is achievable.

IV. CONCLUSIONS

The HC technique was applied to produce SC turbine blades featuring an overhanging shroud usually prone to isolated undercooling and, hence, to grain defects. Because of its excellent thermophysical properties, graphite is recommended as HC material. Numerical simulation and temperature measurements have demonstrated that the application of HC can greatly enhance the cooling condition in the critical region. Maximum undercooling and the corresponding time factor at the outer corner can be significantly reduced. Consequently, structural investigation shows that using the HC technique greatly reduces grain defects. With no HC, most blades cast feature high-angle boundaries and reject-level grain defects. Application of HCs entirely eliminates such defects, and all blades cast are acceptable. This provides confirmation of the effectiveness of the HC technique in improving casting quality.

ACKNOWLEDGMENTS

This work was supported by the Deutsche Forschungsgemeinschaft (DFG). Appreciation is extended to J. Norminikat and R. Weiergräber for their assistance in the experiments and to J. Scheele and R. Laqua, ACCESS e.V. Aachen, for their help in the computer simulation.

REFERENCES

1. B.B. Seth: in *Superalloys 2000*, T.M. Pollock, R.D. Kissinger, R.R. Bowman, K.A. Green, M. McLean, S.L. Olson, and J.J. Schirra, eds., TMS, Warrendale, PA, 2000, pp. 3–6.
2. D.A. Ford and J. Wallbank: *Int. J. Cast Metals Res.*, 1998, vol. 11, pp. 23–28.
3. M. Meyer ter Vehn, D. Dedecke, U. Paul, and P.R. Sahn: in *Superalloys 1996*, R.D. Kissinger, D.J. Deye, D.L. Anton, A.D. Cetel, M.V. Nathal, T.M. Pollock, and D.A. Woodford, eds., TMS, Warrendale, PA, 1996, pp. 471–79.
4. D. Ma and A. Bührig-Polaczek: Patent DE 102007014744, 2007.
5. D. Ma and A. Bührig-Polaczek: *Int. J. Cast Metals Res.*, 2009, in press.
6. K. Harris, G.L. Erickson, R.E. Schwer, J. Wortmann, and D. Froschhammer: “Development of low density single crystal superalloy CMSX-6,” *TMS AIME Fall Meeting*, Detroit, MI, Sept. 17, 1984.
7. P. Sahn, W. Richter, and F. Hediger: *Giesserei-Forschung*, 1983, vol. 35, pp. 35–42.
8. N. Hofmann, U. Reske, H. Vor, and P. Sahn: *Giesserei-Forschung*, 1991, vol. 43, pp. 101–06.
9. A. Ludwig, I. Steinbach, N. Hofmann, M. Balliel, M. van Woerkom, and P.R. Sahn: in *Modelling of Casting, Welding and Advanced Solidification Processes VI*, T.S. Piwonka, V. Voller, and L. Katgerman, eds., TMS, Warrendale, PA, 1993, pp. 87–94.

10. T.M. Pollock, W.H. Murphy, E.H. Golgman, D.L. Uram, and J.S. Tu: in *Superalloys 1992*, S.D. Antolovich and R.W. Stusrud, eds., TMS, Warrendale, PA, 1992, pp. 125–34.
11. I. Wagner and P.R. Sahm: in *Superalloys 1996*, R.D. Kissinger, D.J. Deye, D.L. Anton, A.D. Cetel, M.V. Nathal, T.M. Pollock, and D.A. Woodford, eds., TMS, Warrendale, PA, 1996, pp. 497–506.
12. S.M. Copley and A.F. Giamei: *Met. Trans.*, 1970, vol. 1, pp. 2193–204.
13. R.F. Singer: *3rd Symposium on Advanced Technologies and Processes for Metals and Alloys*, Frankfurt, Germany, 1995.
14. C.R. Hugo: Patent DE 197 30 637 A1, 1997.
15. L. Kats, M. Konter, J. Rösler, and V.P. Lubenets: Patent DE 195 39 770 A1 and US 5.921.310, 1995.
16. K.E. Kats and N. Hofmann: in *Superalloys 2000*, T.M. Pollock, R.D. Kissinger, R.R. Bowman, K.A. Green, M. McLean, S.L. Olson, and J.J. Schirra, eds., TMS, Warrendale, PA, 2000, pp. 189–200.